P2Y$_1$ Antagonists: Combining Receptor-Based Modeling and QSAR for a Quantitative Prediction of the Biological Activity Based on Consensus Scoring

Stefano Costanzi,[*,†] Irina G. Tikhonova,[†] Michihiro Ohno,[‡] Eun Joo Roh,[‡] Bhalchandra V. Joshi,[‡] Anny-Odile Colson,[†] Dayle Houston,[§] Savitri Maddileti,[§] T. Kendall Harden,[§] and Kenneth A. Jacobson[*,‡]

Laboratory of Biological Modeling and Molecular Recognition Section, National Institute of Diabetes and Digestive and Kidney Diseases, NIH, Bethesda, Maryland 20892, and Department of Pharmacology, School of Medicine, University of North Carolina, Chapel Hill, North Carolina 27599

P2Y$_1$ is an ADP-activated G protein-coupled receptor (GPCR). Its antagonists impede platelet aggregation *in vivo* and are potential antithrombotic agents. Combining ligand and structure-based modeling we generated a consensus model (LIST-CM) correlating antagonist structures with their potencies. We docked 45 antagonists into our rhodopsin-based human P2Y$_1$ homology model and calculated docking scores and free binding energies with the Linear Interaction Energy (LIE) method in continuum-solvent. The resulting alignment was also used to build QSAR based on CoMFA, CoMSIA, and molecular descriptors. To benefit from the strength of each technique and compensate for their limitations, we generated our LIST-CM with a PLS regression based on the predictions of each methodology. A test set featuring untested substituents was synthesized and assayed in inhibition of 2-MeSADP-stimulated PLC activity and in radioligand binding. LIST-CM outperformed internal and external predictivity of any individual model to predict accurately the potency of 75% of the test set.

Introduction

P2Y receptors are a family of nucleotide-activated G protein-coupled receptors (GPCRs). Eight subtypes, divided into two subgroups, have been identified in human: the P2Y$_1$ subgroup encompasses P2Y$_1$, P2Y$_2$, P2Y$_4$, P2Y$_6$, and P2Y$_{11}$, which couple to the stimulation of PLC through G$_q$, while the P2Y$_{12}$ subgroup encompasses P2Y$_{12}$, P2Y$_{13}$, and P2Y$_{14}$, which couple to the inhibition of adenylyl cyclase through G$_i$. The two subgroups differ significantly in overall sequence similarity and in their proposed mechanisms of ligand recognition. Natural ligands of the P2Y receptors include ATP, ADP, UTP, UDP, and UDP-glucose.[1,2]

The P2Y$_1$ and P2Y$_{12}$ receptors have both been identified in platelets, where their activation by adenosine diphosphate (ADP, **1a**) mediates a proaggregatory response through different pathways. Activation of P2Y$_1$ leads to shape change and rapid aggregation, while activation of P2Y$_{12}$ causes amplification of the response and sustained aggregation.[3,4] Synergistic activation of both receptors is required to induce ADP-mediated platelet aggregation. Thus, antagonizing each subtype separately has antithrombotic effects. Antagonism of the P2Y$_{12}$ receptor is a validated target in antithrombotic therapy, with the widespread use of the selective antagonist clopidogrel, which acts through a metabolite that irreversibly binds to the P2Y$_{12}$ receptor.[5] Recently, the P2Y$_1$ receptor has been investigated in the same therapeutic context, based on pharmacological studies using both novel ligands and genetic deletion of the P2Y$_1$ receptor in mice.[6]

While ADP (**1a**) is the natural agonist, adenosine 3′,5′-bisphosphate (A3P5P, **1b**) was found to act as a competitive antagonist of the human P2Y$_1$ receptor (Chart 1).[7] Since then,

we have extensively investigated the structure−activity relationships (SAR) of A3P5P derivatives.[8−15] The compounds which were synthesized and tested include also acyclic derivatives, such as **2**, in which the ribose is substituted with acyclic moieties,[11,12] and conformationally locked derivatives, such as **3a**, **3b** (MRS2279), and **3c** (MRS2500).[12−14] In the latter derivatives, the ribose is replaced with a bicyclo[3.1.0]hexane ring, also known as a Northern (N)-methanocarba ring system, which constrains the pseudosugar in the 2′-exo conformation which is preferred by the receptor binding site. These derivatives are competitive in binding and several have been shown to be useful as tracers in radioactive form.[16] Compound **3c** was shown to be effective in reducing thrombus formation in vivo and to be more resistant to degradation than the related 9-riboside derivatives.[6]

In the present work, we combined receptor-based modeling and QSAR (quantitative structure−activity relationships) methodologies in the attempt to generate models capable of correlating the chemical structures of P2Y$_1$ antagonists with their biological activities. Such models would be of great assistance in the drug discovery process, as the activity of new compounds could be estimated in a quantitative manner before their synthesis and testing.

Since a crystal structure is available only for bovine rhodopsin in the GPCR family,[17] we developed rhodopsin-based molecular models of the P2Y$_1$ receptor.[1,11] Subsequently, we studied the interactions of competitive antagonists with the putative binding site of the receptor with an iterative approach which included flexible molecular docking, mutagenesis, and chemical modification of the ligands.[1,11,14,18]

Docking scores alone are not a viable route for the prediction of the affinity of new ligands and cannot be applied to the lead optimization process.[19,20] This is especially true when the structure of the receptor is inferred by homology modeling rather than being experimentally determined. However, experimentally supported docking models reliably provide the bioactive conformation of the ligands and their binding modes into the

---

* Corresponding authors. (S.C.) Email: stefanoc@mail.nih.gov. Phone: 301-451-7353. Fax: 301-480-4586. (K.J.) Email: kajacobs@helix.nih.gov. Phone: 301-496-9024. Fax: 301-480-8422.
† Laboratory of Biological Modeling, National Institute of Diabetes and Digestive and Kidney Diseases.
‡ Molecular Recognition Section, National Institute of Diabetes and Digestive and Kidney Diseases.
§ University of North Carolina, Chapel Hill.

Chart 1

1a, ADP

1b, A3P5P

2,MRS 2298

3a X = H, **MRS2275**
3b X = Cl, **MRS2279**
3c X = I, **MRS2500**
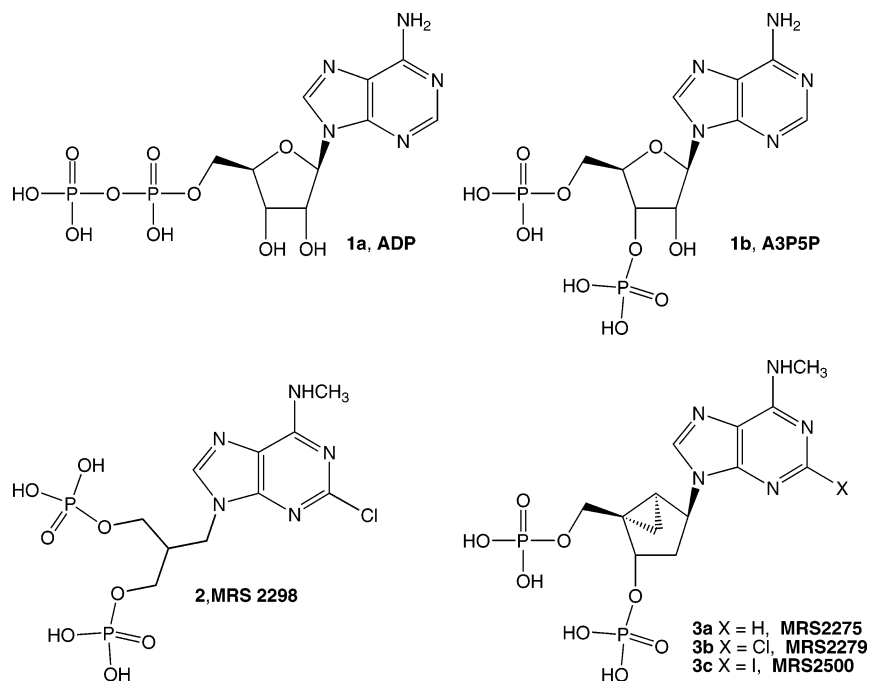
receptor binding pockets.[19,21] Here we used the structural alignment and the bioactive conformations resulting from docking for the construction of QSAR models based either on molecular fields or on molecular descriptors. Subsequently, in order to benefit from the strength of each individual technique, we combined the models based on receptor−ligand interactions and those based on QSAR to generate a PLS model based on consensus scoring.

To validate our consensus model, we assayed the antagonistic potency of 8 analogues of A3P5P (**1b**), 7 of which were newly synthesized, in the methanocarba and acyclic series. The compounds were also tested for their binding affinity. In parallel with the experimental measurements, we predicted theoretically the potency of the new compounds. Finally, experimental and theoretical values were compared to assess the predictive capabilities of our models.

Throughout this paper (a) the statistical models linking the biological activities (dependent variables) to the molecular properties (independent variables) were always built by means of partial least-square (PLS) regressions, (b) the degree of correlation of experimental versus predicted activities was always expressed in terms of the square of the correlation coefficient (r^2), which indicates the fraction of explained variance, (c) the internal predictivity was always measured in terms of cross-validated r^2 (q^2), after cross-validation with the leave-one-out method, and (d) to facilitate the comparison among receptors, we used the GPCR residue indexing system as explained elsewhere.[1]
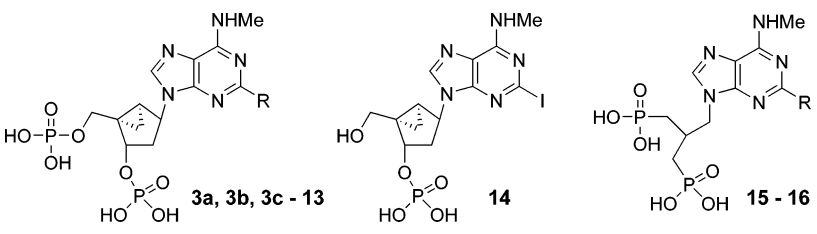
Results

The Training Set. We collected 45 P2Y$_1$ antagonists published by our group between 1998 and 2004. The antagonistic properties of all the compounds have been tested, in the course of the years, in the laboratory of T. Kendall Harden for the inhibition of the phospholipase C (PLC) activity stimulated by 2-MeSADP.[8−11,13,14] The 45 compounds are all A3P5P (**2**) analogues and encompass ribose derivatives, anhydrohexitol derivatives, acyclic derivatives, (N)-methanocarba derivatives, and bicyclo[2.2.1]heptane derivatives. They are all characterized

by the presence of two monophosphate groups and bear various substitutions at the purine ring. The compounds are endowed with potencies ranging from low nM to high μM. The most potent is the (N)-methanocarba analogue **3c**, which shows an IC$_{50}$ of 8.4 nM in inhibition of PLC activity and a K_i of 0.78 nM in binding studies (Table 1).[14] A table reporting the structures of all the compounds in the training set, their potencies, and references to the original publications is supplied as Supporting Information (Table S1).

Receptor-Based Molecular Modeling. We refined our model of the P2Y$_1$−**3c** complex by means of a cycle of Monte Carlo Multiple Minima (MCMM)[22] conformational analysis granting full flexibility to the ligand and to the residues forming the binding cavity (Figure 1a). Consistently with our previous reports, the phosphates are coordinated by three cationic residues located in TM3, TM6, and TM7, namely R128(3.29), K280-(6.55), and R310(7.39), which proved fundamental for the recognition of agonists and antagonists. The amino group at the 6 position of the purine ring (N^6) donates a hydrogen-bond (H-bond) to Q307(7.36), while the nitrogen at the 1 position (N1) accepts an H-bond from S314(7.43).

After the optimization of the P2Y$_1$ model around **3c**, we automatically docked into the receptor each of the 45 compounds of the training set. The docking experiments have been performed by means of the Glide[23] module of the Schrödinger package granting full flexibility to the ligands. The receptor was treated as a rigid grid with softened van der Waals (vdW) potentials. To account for the flexibility of the receptor and induced fit phenomena, we submitted the docking complexes to an energy minimization cycle by means of the Liaison[23] module of the Schrödinger package and subsequently recalculated the docking scores (LiaScore). The highest scoring poses of the training set compounds aligned very well inside the P2Y$_1$ binding cavity, establishing with the receptor the characteristic interactions proposed by our experimentally supported model (Figure 1b).

Overall, the PLS regression of LiaScore resulted in predicted potencies which did not significantly deviate from the experimental potencies, as indicated by a root-mean-square error

Table 1. In Vitro Pharmacological Data at the Human P2Y$_1$ Receptor for Inhibition of Radioligand Binding and for Inhibition of PLC Activity Stimulated by 2-MeSADP

compound	R	binding, K_i, nM[a,c]	antagonism, IC$_{50}$, nM[b−d]
3a[e]	H	17.6 ± 2.7[13]	157 ± 60[13]
3b[e]	Cl	2.5 ± 0.4[13]	52 ± 1[13]
3c[e]	I	0.78 ± 0.08[13]	8.4 ± 0.8[13]
4	SCH$_3$	91 ± 12[13]	221 ± 30[13]
5[f]	CN	540 ± 133	6900 ± 2500
6[f]	CONH$_2$	650 ± 266	1750 ± 1100
7[f]	CO$_2$H	1430 ± 930	870 ± 180
8	CH$_3$	3.6 ± 0.7[13]	48 ± 1[13]
9	(CH$_2$)$_5$CH$_3$	80 ± 10[13]	452 ± 221[13]
10	*trans*-CH=CH(CH$_2$)$_3$CH$_3$	330 ± 70[13]	1870 ± 590[13]
11[e,f]	C≡CH	95 ± 39	93 ± 30
12	C≡C(CH$_2$)$_3$CH$_3$	430 ± 200[13]	2400 ± 600[13]
13[f]	C$_6$H$_5$	273 ± 26	1940 ± 1000
14[f]		706 ± 219	1560 ± 540
15[f]	Cl	76 ± 10[15]	620 ± 40
16[e,f]	I	66 ± 12	790 ± 1600

[a] Affinities determined by using [³H]**3b** in a radioligand binding assay. The human P2Y$_1$ receptor was expressed to high levels in Sf9 insect cells with a recombinant baculovirus. Membranes prepared from these cells were incubated for 30 min at 4 °C in the presence of ∼20 nM [³H]**3b**. [b] Antagonist IC$_{50}$ values represent the concentrations needed to inhibit by 50% the effect elicited by 100 nM 2-MeSADP on the human P2Y$_1$ receptor expressed in 1321N1 astrocytoma cells. [c] Mean ± SEM given for three separate determinations. [d] None of the compounds displayed agonist effects. [e] **3a**, MRS2275; **3b**, MRS2279; **3c**, MRS2500; **11**, MRS2611; **16**, MRS2609. [f] Test set compounds.

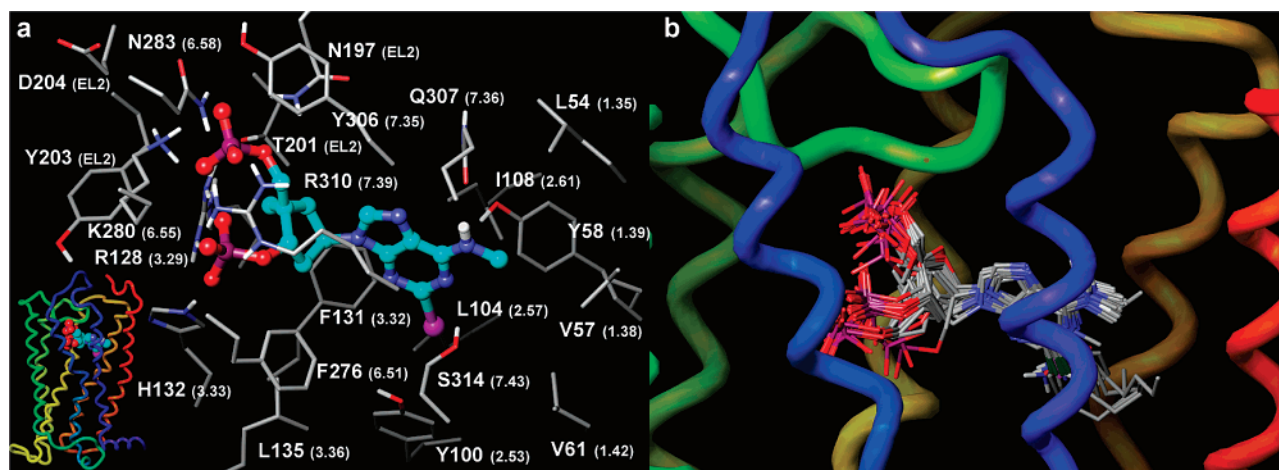**Figure 1.** (a) Details of the P2Y$_1$ receptor binding site complexed with the antagonist **3c** as obtained after fully flexible Monte Carlo conformational search. A schematic representation of the receptor−ligand complex is given in the lower left inset. (b) Docking complexes of the P2Y$_1$ receptor and the 45 compounds of the training set. In the tube representations the receptor is colored according to residue positions, with a spectrum of colors that ranges from red (N-terminus) to purple (C-terminus): TM1 is in orange, TM2 in ochre, TM3 in yellow, TM4 in green, TM5 in cyan, TM6 in blue, TM7 in purple.

(RMSE) of 0.660. Thus, the molecules in the training set were recognized as binders and their potencies were estimated with a reasonably low error. However, the LiaScore model clearly appeared unable to rank the compounds according to their potency, as indicated by r^2 and q^2 values close to 0 (Table 2). We also calculated the free energy of binding based on the linear interaction energy method (LIE), also known as linear response method (LRM),[24,25] in a surface generalized Born (SGB) continuum model for solvation as implemented in Liaison.[26−28] The calculation, which relied on energy minimizations, yielded a PLS model showing a lower RMSE and a significant improvement of correlation and internal predictivity (Table 2).

However, with a q^2 of 0.317 the model certainly did not offer the reliability necessary to estimate the potency of novel compounds.

Docking-Based QSAR: (a) Molecular Fields. Comparative molecular fields analysis (CoMFA) and comparative molecular similarity indices analysis (CoMSIA) are 3D-QSAR methods intended to correlate the molecular features of a series of compounds with their biological activities. CoMFA and CoMSIA do not take into account receptor−ligand interactions but rely only on the calculation of the molecular fields of the ligands and their subsequent correlation, by PLS regression, to their biological activities. In particular, CoMFA is based on the calculation

Table 2. PLS Statistics for the Predictions of the Antagonistic Potency of the Training Set Compounds. Plots of Experimental vs Calculated Potencies for the Training Set Compounds Are Available as Supporting Information (Figure S1)

method	$r^{2\,a}$	$q^{2\,b}$	RMSE^c
LiaScore	0.080	0.017	0.660
SGB-LIE	0.441	0.317	0.514
CoMFA	0.904	0.590	0.229
CoMSIA	0.815	0.513	0.314
MOE 2D	0.766	0.372	0.573
MOE 3D	0.690	0.563	0.383
MOE 2D and 3D	0.876	0.688	0.243
consensus	0.922	0.890	0.192

^{a} Square of the correlation coefficient. ^{b} Cross-validated square of the correlation coefficient (leave-one-out method). ^{c} Root-mean-square error (RMSE) in the non cross-validated analysis.

of steric and electrostatic fields, while CoMSIA considers also hydrophobic, H-bond acceptor, and H-bond donor fields.

In order to provide meaningful models, CoMFA and CoMSIA are dependent on knowledge of the bioactive conformation of the ligands and of their relative structural alignment. Here we derived this information directly from our docking studies, thus generating docking-based 3D-QSAR models.

When compared to docking scores and SBG-LIE calculations, the PLS analysis of our docking-based CoMFA ($r^2 = 0.904$; $q^2 = 0.590$) and CoMSIA ($r^2 = 0.815$; $q^2 = 0.513$) appeared statistically more robust and showed a significantly higher internal predictivity. The optimal number of components was found to be 5 for CoMFA and 4 for CoMSIA.

Since the QSAR models were built on the basis of docking, we could dock the 3D molecular fields produced by CoMFA and CoMSIA into the receptor binding pocket, thus evaluating the complementarity of the ligand-based QSAR and our proposed model of the ligand−receptor interactions. The
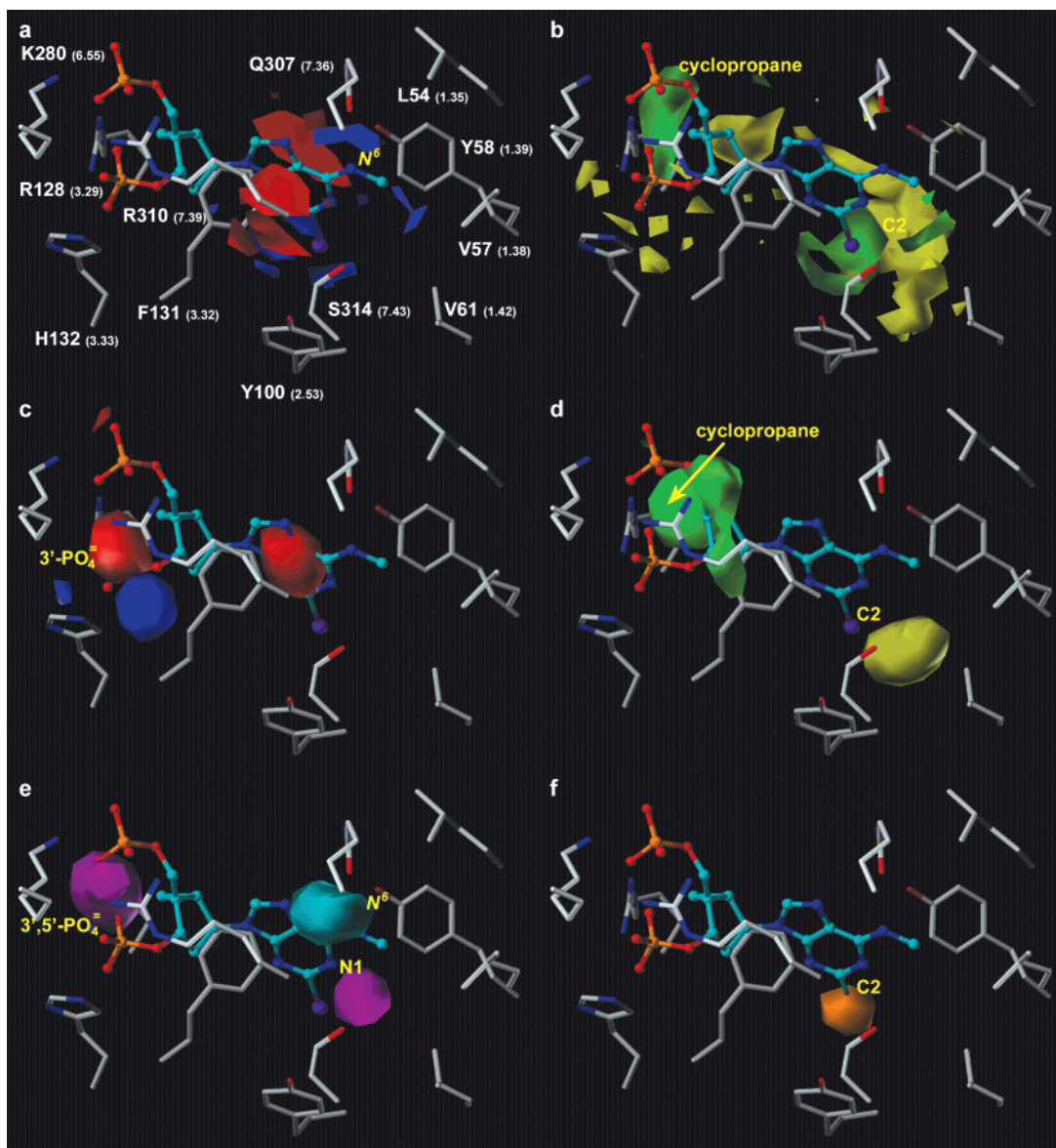

Figure 2. Contour maps of the CoMFA and CoMSIA models (StDev*Coeff) docked into the P2Y$_1$ binding site. Compound **3c** is shown as a representative antagonist. The moieties of the antagonists responsible for the productions of the molecular fields are labeled in yellow. (a) CoMFA electrostatic fields: positive charges increase the potency in the blue areas and decrease it in the red areas (contour levels 90% and 20%). (b) CoMFA steric fields: bulky substituents increase the potency in the green areas and decrease it in the yellow areas (contour levels 80% and 20%). (c) CoMSIA electrostatic fields: positive charges increase the potency in the blue areas and decrease it in the red areas (contour levels 90% and 20%). (d) CoMSIA steric fields: bulky substituents increase the potency in the green areas and decrease it in the yellow areas (contour levels 90% and 20%). (e) CoMSIA H-bond fields: H-bond donors increase the potency in the cyan areas, while H-bond acceptors increase it in the magenta areas (contour levels 85%). (f) CoMSIA hydrophobic fields: hydrophobic substituents increase the potency in the orange areas (contour levels 85%).

electrostatic fields suggest the importance of the aromaticity of the purine ring, which binds in a region surrounded by aromatic residues (Figure 2a and 2c, red fields). The N^6 group shows electrostatic (CoMFA, Figure 2a, blue field) or H-bond (CoMSIA, Figure 2e, cyan field) interactions with the essential residue Q307(7.36). The N1 produces a strong H-bond acceptor field corresponding to S314(7.43) (CoMSIA, Figure 2e, magenta field). H-bond donor fields are detected by CoMSIA in proximity of the phosphate groups and are complemented in the receptor model by the three critical cationic residues R128-(3.29), K280(6.55), and R310(7.39), and by H132 (3.33) (Figure 2e, magenta field). The latter is characteristic of P2Y₁ and may contribute to the selectivity of A3P5P analogues for this subtype. In agreement with the arrangement of the cationic residues, CoMSIA distinguishes between the orientations of the 3′-phosphate that are beneficial (Figure 2c, red field) or detrimental (Figure 2c, blue field) for the potency. Since all the studied ligands are A3P5P analogues, CoMFA does not reveal the contribution of the phosphates to the potency of the compounds. If we add to the training set an analogue of **3c** without the phosphates (i.e., 2-iodo-N^6-methyl-2′-deoxyadenosine) and we assume the compound to be inactive, strong electrostatic fields are produced in the regions corresponding to the phosphates (Supporting Information, Figure S2c, lower right inset). CoMFA and CoMSIA suggest that at the 2 position small substituents are beneficial (Figure 2b, green fields, and Figure 2f, orange field), while large groups, which cause steric clashes with residues in TM1 and TM2, are not tolerated (Figure 2b and 2d, yellow fields). Finally, CoMFA and CoMSIA reveal the positive effect of the cyclopropane ring of the methanocarba pseudosugar (Figure 2b and 2d, green fields). This is not due to a favorable interaction with the binding site but to the locked Northern conformation induced by the methanocarba system.

Docking-Based QSAR: (b) Molecular Descriptors. Alternatively, using the QSAR applications of the molecular operating environment (MOE 2005),[29] we have calculated 184 2D descriptors and 67 3D descriptors for the compounds of the training set. While 2D descriptors do not depend on the conformation of the molecules, 3D descriptors are always conformation-dependent and, in some cases, alignment-dependent. Also in this case, we made use of the putative bioactive conformations and the 3D alignment of the molecules resulting from the docking studies.

We identified the 16 2D descriptors and 10 3D descriptors that best correlate with the potency of the training set compounds. In particular, the 2D descriptors included subdivided surface areas, Kier and Hall connectivity indices, and six different physical properties, while the 3D descriptors included conformation-dependent charge descriptors as well as surface area and shape descriptors (Table 3).

PLS analysis (Table 2) showed that use of the 3D descriptors alone (q² = 0.563) yielded a higher internal predictivity than 2D descriptors alone (q² = 0.372). However, the best result was obtained from the combination of 2D and 3D descriptors (q² = 0.688).

Combining QSAR and Docking Scores in a Ligand and Structure-Based Consensus Model (LIST-CM). Combining the scores obtained with different methodologies may result in a significant improvement of the predictivity over the individual techniques (see Discussion). Thus, we treated the predictions obtained with the individual methodologies as independent descriptors and correlated them to the potency of the compounds through PLS regression, generating a consensus model (LIST-CM) based on LiaScore, SGB-LIE, CoMFA, CoMSIA, MOE

Table 3. Description and Relative Weight of the Molecular Descriptors Used To Build the QSAR Model. All the Descriptors Were Calculated with the QSAR Applications in MOE 2005[29,38]

weight	name[a]	description[a]
2D Physical Properties		
0.005353	mr	molecular refractivity
0.082981	AM1_HF	AM1 heat of formation
0.173345	PM3_HOMO	PM3 energy of the HOMO
0.005953	SlogP	log of the octanol/water partition coefficient[39]
0.211838	TPSA	polar surface area with group contributions[40]
0.016101	logS	log of the aqueous solubility[41]
2D Subdivided Approximate van der Waals Surface Areas[38]		
0.215821	SlogP_VSA0	
0.077908	SlogP_VSA1	
0.430744	SlogP_VSA2	
0.260983	SlogP_VSA3	
0.135706	SlogP_VSA4	
0.276779	SlogP_VSA5	
0	SlogP_VSA6[b]	
0.221864	SlogP_VSA7	
0.735487	SlogP_VSA8	
0.352781	SlogP_VSA9	
2D Kier and Hall connectivity		
0.018255	chi0	atomic connectivity index (order 0)[42]
3D Surface Area and Shape Descriptors		
0.241597	ASA	water accessible surface area
0.080319	pmiX	x component of the principal moment of inertia
0.49167	pmiY	y component of the principal moment of inertia
0.205061	pmiZ	z component of the principal moment of inertia
1	VSA	van der Waals surface area
3D Conformation Dependent Charge Descriptors		
0.053425	ASA_H	water accessible surface area of hydrophobic atoms
0.059199	ASA_P	water accessible surface area of polar atoms
0.04164	dipole X	x component of the dipolar moment
0.013659	dipole Y	y component of the dipolar moment
0.012961	dipole Z	z component of the dipolar moment

[a] More details on the descriptors are available at: http://www.chemcomp.com/journal/descr.htm. [b] SlogP_VSA6 was 0 for all the compounds in the training set and was not used in the PLS analysis.

QSAR with 2D descriptors, MOE QSAR with 3D descriptors, and MOE QSAR with 2D and 3D descriptors. Remarkably, the consensus model resulted in significantly more robust statistics (Table 2). Notably, with a q² of 0.890, this model showed an internal predictivity superior to that of any individual methodology.

The Test Set. To measure the external predictivity of our models, we chose a particularly challenging test set of eight compounds to be synthesized and tested biologically, each of which showed at least one substituent not featured in the training set.

The eight compounds of the test set belong either to the methanocarba or to the acyclic series (Table 1, compounds **5**, **6**, **7**, **11**, **13**, **14**, **15**, **16**). In particular, six compounds are analogues of **3c** bearing different substituents at the 2 position or lacking the 5′-phosphate, while the 2 remaining compounds belong to the acyclic series and bear phosphonate groups at the 3′ and 5′ positions. To avoid any bias in the construction of the models, the potencies of the compounds were quantitatively predicted before the compounds were tested.

The Test Set: Synthesis. The (N)-methanocarba bisphosphate analogues **5**−**7**, **11**, and **13** were synthesized using a Mitsunobu reaction to combine adenine and bicyclohexane moieties.[13,15,30] The functional group at the 2 position was formed by both prefunctionalization of the adenine moiety and later manipulation following condensation with the pseudoribose ring. The cyano group was introduced by the reaction of zinc cyanide on the corresponding 2-iodo intermediate **17** using palladium chemistry in tetramethylurea (Scheme 1).[14] The Pd-(0) complex was generated in situ from tri-(2-furyl)phosphine
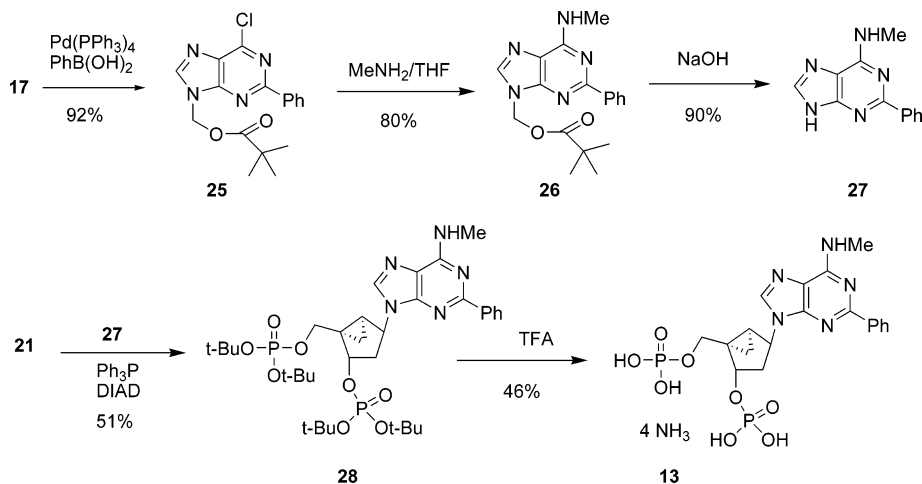
Scheme 1
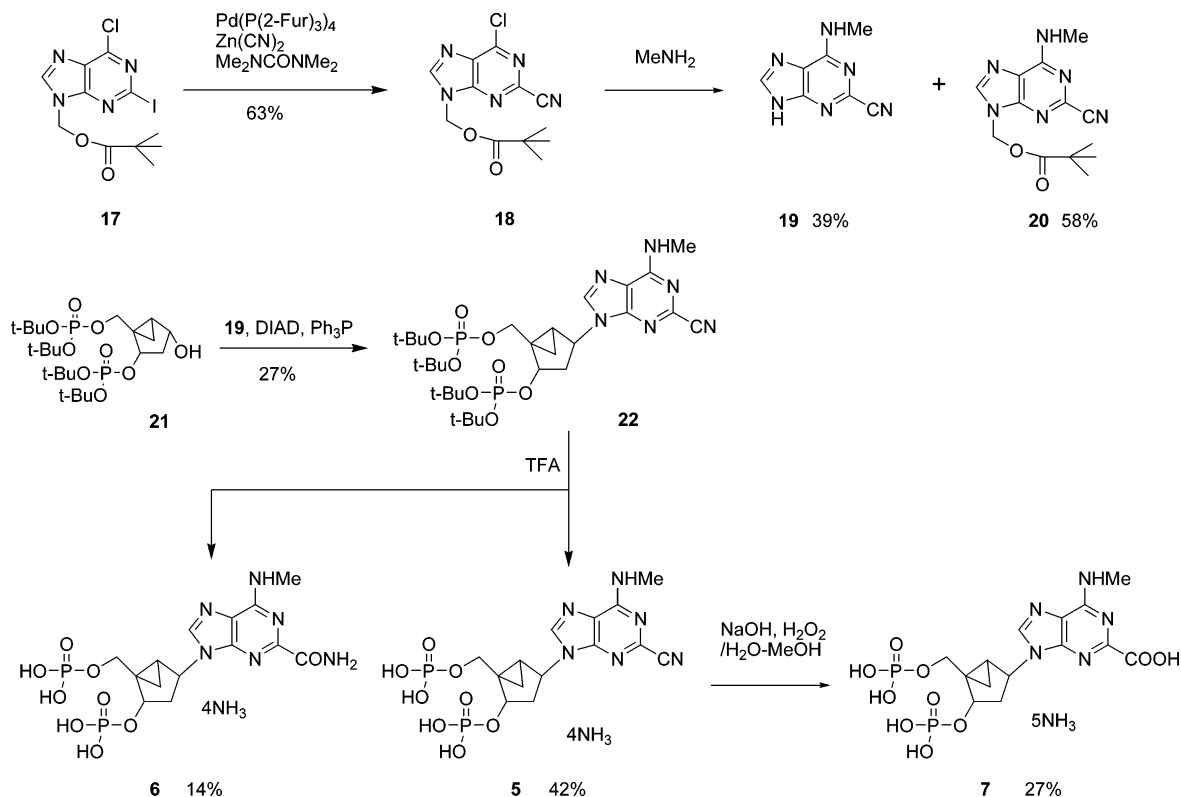
Scheme 2
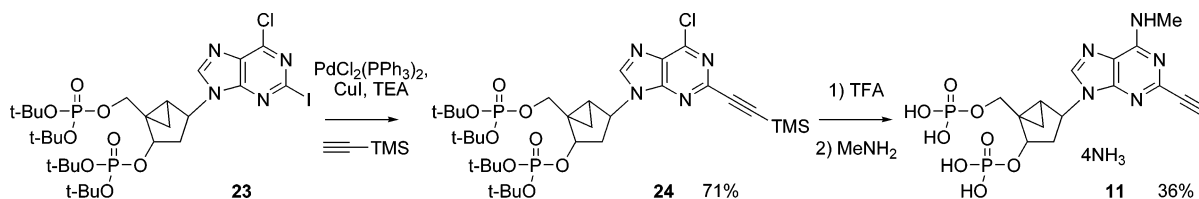
Scheme 3


and Pd$_2$(dba)$_3$ (tris(dibenzylideneacetone)dipalladium(0) chloroform adduct). The cyano group was later converted in TFA to the carboxamide **6** or hydrolyzed to give the carboxylic acid derivative **7**. A 2-iodo intermediate reacted with trimethylsilyl-acetylene followed by deprotection to provide **11** (Scheme 2). A 2-phenyladenine intermediate **25** was generated by a Suzuki coupling reaction followed by introduction of the N^6-Me group, deprotection at the 9 position, condensation with the prephosphorylated bicyclic ring system, and final deprotection to yield

13 (Scheme 3). To probe the need for bisphosphorylation, the 5′-hydroxyl analogue **14** was prepared using a selective alcohol protection approach with phosphorylation and deprotection as the final steps (Scheme 4). Compound **14** also served as a precursor for the enzymatic synthesis of a radiolabeled form of **3c**.[16]

The synthesis of acyclic phosphonate derivative **16** (Scheme 5) started with coupling of 2-iodo-6-chloro purine[12,31] with the alcohol[15] **36** by a Mitsunobu reaction to afford **37** in 52% yield.

Scheme 4
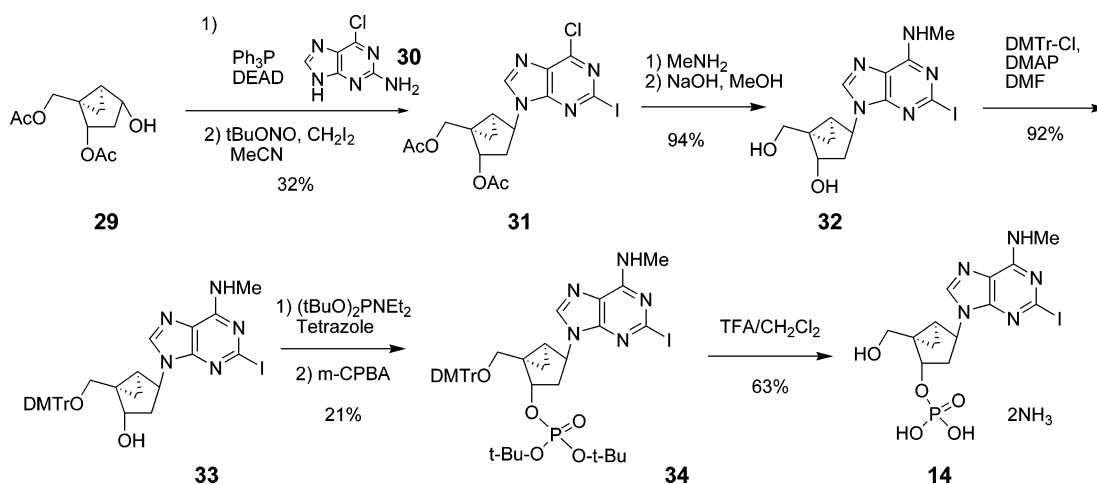
Scheme 5
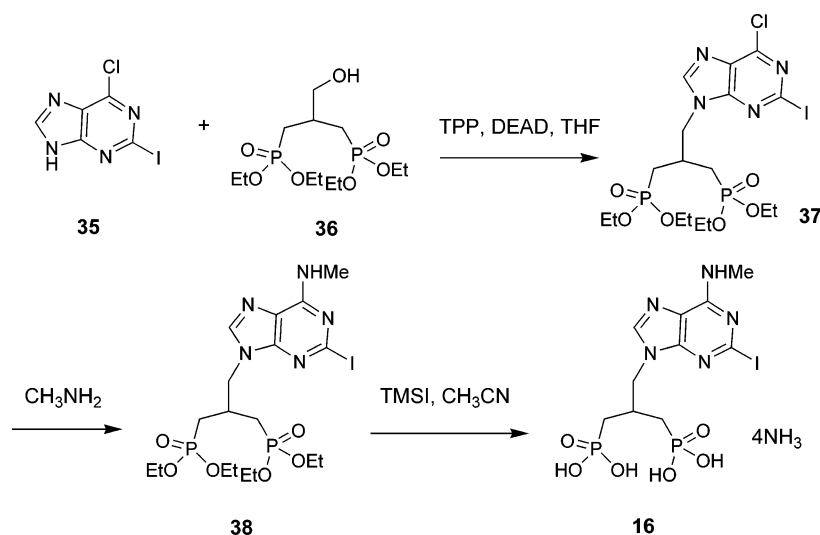
The displacement of the 6-chloro group with methylamine followed by treatment with excess of iodotrimethylsilane afforded the requisite 2-iodo phosphonate analogue **16**.

The Test Set: Pharmacological Activity. Unlike 2-halo substituents, the cyano moiety and polar carboxy and carboxamido substituents at the 2 position (**5**−**7**, Table 1) were poorly tolerated by the P2Y₁ receptor. Interestingly, among these three new molecules, compound **5**, which bears the 2-cyano substituent, showed the highest binding affinity but the lowest antagonistic potency, while the opposite happened for **7**, which bears the 2-carboxy substituent.

The 2-ethynyl-substituted compound **11** proved to have higher affinity and potency than the corresponding compound **12**, which bears a longer hexynyl chain. This is consistent with the previously observed tendency of the P2Y₁ receptor to prefer small substituents at the 2 position, as in **8**, rather than larger chains, as in **9**, **10** or **12**.[13] This trend also appears evident upon analysis of the CoMFA and CoMSIA steric contours (Figure 2b and 2d). Consistently, the 2-phenyl-substituted compound **13** showed lower affinity and potency than the less bulky compound **11**.

In compound **14**, the removal of the 5′-phosphate group of **3c** led to a great loss in affinity and potency.

In the acyclic phosphonate series, the 2-iodo substituent of **16** was well tolerated, showing affinity and potency similar to those of the corresponding 2-chloro derivative **15**. Thus, it did

not lead to a more potent inhibitor as it did in the (N)-methanocarba series.

The Test Set: Prediction and Validation. The predicted antagonistic potencies of the compounds in the test set, expressed as pIC₅₀, are reported in Table 4. Plots of experimental versus predicted potencies for the test set compounds, together with a synoptic bar graph representation, are given as Supporting Information (Figures S3 and S4).

The root-mean-square error of prediction (RMSEP) proved to be low for all the methodologies. Thus, all compounds were correctly recognized as P2Y₁ antagonists. However, none of the models showed good ranking capabilities over the whole test set, measured in terms of r^2.

All the methodologies showed outliers, defined as compounds with an error of prediction higher than 1 log unit. In particular, the LiaScore model showed only 1 outlier and proved to be the methodology endowed with the lowest RMSEP. Thus, the LiaScore model proved to be the methodology least affected by the structural diversity.

On the other side of the spectrum, the MOE descriptor-based QSAR proved to be very dependent on the structures of the compounds included in the training set. Six test set compounds were outliers for the model based on 2D and 3D descriptors. These are all molecules that bear functionalities very distant from those present in the training set: compound **11** bears an alkynylic chain significantly shorter than those included in the

Table 4. Prediction of the Antagonistic Potencies of the Compounds in the Test Set. Errors of Predictions Are Shown in Parentheses

	experimental	consensus	LiaScore	SGB-LIE	CoMFA	CoMSIA	MOE 2D	MOE 3D	MOE 2D and 3D
					pIC50 in inhibition of 2-MeSADP stimulated PLC activity				
5	5.16	5.66	6.19	6.62	7.15	6.84	10.10	2.91	4.42
		(0.50)	(1.03)	(1.46)	(1.99)	(1.68)	(4.94)	(−2.25)	(−0.74)
6	5.76	6.02	6.32	6.91	6.89	5.52	6.66	3.87	4.19
		(0.26)	(0.56)	(1.15)	(1.13)	(−0.24)	(0.90)	(−1.89)	(−1.57)
7	6.06	6.15	5.98	6.95	7.26	6.45	4.65	3.64	3.48
		(0.09)	(−0.08)	(0.89)	(1.20)	(0.39)	(−1.41)	(−2.42)	(−2.58)
11	7.03	6.76	6.25	6.68	6.96	6.50	3.65	6.23	5.33
		(−0.27)	(−0.78)	(−0.35)	(−0.07)	(−0.53)	(−3.38)	(−0.80)	(−1.70)
13	5.71	5.99	6.49	6.56	6.18	6.41	6.44	7.11	6.01
		(0.28)	(0.78)	(0.85)	(0.47)	(0.70)	(0.73)	(1.40)	(0.30)
14	5.81	6.47	4.94	1.82	5.52	7.23	6.81	10.33	9.97
		(0.66)	(−0.87)	(−3.99)	(−0.29)	(1.42)	(1.00)	(4.52)	(4.16)
15	6.21	7.54	5.73	5.66	6.50	6.50	3.90	7.07	7.96
		(1.33)	(−0.48)	(−0.55)	(0.29)	(0.29)	(−2.31)	(0.86)	(1.75)
16	6.10	7.78	5.74	6.08	6.69	6.83	4.98	7.52	8.55
		(1.68)	(−0.36)	(−0.02)	(0.59)	(0.73)	(−1.12)	(1.42)	(2.45)
RMSEP		0.83	0.68	1.63	0.96	0.90	2.42	2.24	2.21
		(0.39)[a]							
r^2		0.30	no correlation	0.01	0.01	no correlation	no correlation	0.07	0.01
		(0.79)[a]							
outliers		2	1	3	3	2	6	6	6

[a] Value obtained excluding compounds **15** and **16** (outliers) from the PLS regression.

training set, compounds **6** and **7** bear a carboxamido and a carboxy substituent at the 2 position, compound **14** bears a 5′-OH group, and compound **15** and **16** bear phosphonate groups. Confirming the dependence of the descriptor-based QSAR from the training set, when either compound **6** or **7** was introduced in the training set, the error of prediction on the other compound was significantly reduced (Supporting Information, Table S2).

Our consensus model (LIST-CM) performed significantly better than any individual methodology also in the evaluation of the potencies of the test set compounds. With a predictive r^2 of 0.30, consensus scoring proved to be the only model able to rank the potencies of the compounds in the test set. Indeed, the potency of six out of the eight new compounds was accurately estimated. Remarkably, if we exclude the two outliers, consensus scoring shows an r^2 of 0.79 and an RMSEP as low as 0.39. Thus, our consensus model accurately and sharply predicted the potency of 75% of the test set compounds.

Discussion and Conclusions

The lack of ranking ability of the PLS regression based purely on receptor−ligand interactions did not surprise us. Docking scores and prediction of the free energy of binding provide a direct estimation of the affinity of the compounds ($\Delta G = RT \ln K_i$). The free energy of binding can also be linked to the IC_{50} with the equation $\Delta G \simeq RT \ln (IC_{50})$, which however stays in place only if the potencies are linearly correlated with the affinities. Although this is expected to generally happen for closely related compounds, the discrepancies between the binding and functional data for our test set suggest that it may not necessarily be the case for the ligands that are the object of our study. The use of binding data in our QSAR analyses was not an option due to the nonavailability of such data for most of the training set. Aside from these considerations, a homology model does not provide a sufficiently high resolution of the binding site to accurately infer the difference in the activities of various compounds.

However, docking scores are powerful tools to handle structurally diverse compounds and to distinguish between binders and nonbinders. In particular, our LiaScore model proved to be essentially independent from the training set.

Furthermore, docking programs provide accurate binding modes and ligand conformations. Here, we used the conformation and the alignment of the ligands obtained in the docking studies to build QSAR models. An advantage of docking-based 3D-QSAR is the possibility of plugging the contour maps into the receptor binding pockets. Thus, we docked the CoMFA and CoMSIA maps into our P2Y$_1$ model, ascertaining good complementarity between the ligand-based 3D contour maps and the molecular features of the receptor.

All of our docking-based QSAR studies yielded very good correlation coefficients and good internal predictivities, which were always higher than those obtained on the basis of docking scores and free binding energy predictions. Notably, the MOE descriptor-based QSAR yielded the highest internal predictivity, as measured by the q^2 value. However, this model appeared very sensitive to the nature of the training set, and its good internal predictivity did not translate into a good external predictivity.

Thus, we merged receptor-based modeling and QSAR by generating a PLS model based on consensus (LIST-CM). Consensus scoring allows combining the strength of the individual methodologies while mitigating their inherent limits. The intrinsic coarseness of the receptor-based scores is compensated by the higher accuracy of the QSAR-based scores. At the same time, the substantial independence of the receptor-based scores from the chemical nature of the compounds in the training set compensates for the limits of the QSAR-based scores. To validate our consensus model, we chose a particularly challenging test set, in which each compound presents at least one feature not included in the training set. Consensus scoring proved to be more robust than any individual model both in terms of internal and external predictivity. Remarkably, consensus scoring predicted with accuracy the potency of 75% of the test set compounds.

Experimental Section

Conformational Search of 3c within the P2Y$_1$ Receptor Binding Pocket. Our previous rhodopsin-based model of the P2Y$_1$ receptor complexed with the antagonist **3c** was subjected to an optimization by fully flexible conformational search with the Monte Carlo Multiple Minimum (MCMM) method,[22] as implemented in

the MacroModel 9.1.[32,33] The search was performed on the ligand and the residues in the binding pocket, defined as the residues located within 6 Å from the ligand. An additional shell of residues located within 3 Å from the binding pocket were included in the calculation, but were conformationally frozen. The following parameters were employed for the conformational search: number of steps = 100; number of structures to save for each search = 100; energy window for saving structures = 1000.0 kJ/mol. The calculations were conducted with the MMFFs force field. For the energy minimizations the Polak−Ribiere Conjugate Gradient was used with a convergence threshold on the gradient of 0.05 kJ/Å/mol.

Automatic Docking. All the compounds of the training and the test sets were automatically docked into the P2Y₁ binding site by means of Glide 4.0.[23] The model of the P2Y₁ receptor optimized with **3c** in the binding pocket obtained as described in the previous paragraph was used for the docking experiments. All the compounds were sketched from **3c**, subjecting any added moiety to energy minimization with the MMFFs force field until a convergence threshold on the gradient of 0.05 kJ/Å/mol was reached with the Polak−Ribiere Conjugate Gradient. In the receptor grid generation, the vdW radii were scaled by 0.75 for the atoms with a partial atomic charge less than 0.25*e*. The docking box was defined as a cube of 10 Å centered on the centroid of the **3c**. The ligands were docked with the extra precision (XP) mode using default settings and scaling by 0.80 the vdW radii of the ligands with partial atomic charge less than 0.15*e*. The docking scoring function (LiaScore) and the linear interaction energy (LIE) were calculated with Liaison in a surface generalized Born continuum model for solvation (SGB).[26] Energy minimization was used as a sampling method, with the Truncated Newton algorithm and with a residue-base cutoff for nonbonded interactions of 15 Å. The OPLS 2005 force field was used. The ligand and the closest residues were treated as fully flexible; residues further than 4 Å from the ligand were restrained, while those further than 7 Å were frozen. LiaScore is essentially the Glide scoring function[23,34] calculated during the Liaison simulation. The LIE-SGB free binding energies were calculated according to the empirical equation:

$$\Delta G = \alpha \left(\langle U^b \text{vdw} \rangle - \langle U^f \text{vdw} \rangle \right) + \beta \left(\langle U^b \text{elec} \rangle - \langle U^f \text{elec} \rangle \right) + \gamma \left(\langle U^b \text{cav} \rangle - \langle U^f \text{cav} \rangle \right)$$

where b indicates the bound form of the ligand, f indicates the free form of the ligand, and U_{cav} represent an energy term proportional to the exposed surface area of the ligand.[26,27]

Prediction of the pIC₅₀ values were obtained by PLS regressions of the LiaScore and the LIE-SGB descriptors, which were performed with the QuaSAR-Model application of MOE using default parameters.[29] Experimental pIC₅₀ values were used as dependent variables.

CoMFA and CoMSIA. A 3D cubic lattice with grid spacing of 1 Å and extending 4 Å behind the aligned molecules in all directions was used. The molecular fields (steric and electrostatic for CoMFA; steric, electrostatic, H-bond donor, H-bond acceptor, and hydrophobic for CoMSIA) were calculated using a probe atom with the vdW properties of an sp3 carbon and with a charge of +1.0. For the generation of the CoMFA fields, a distance dependent dielectric was selected for Coulombic electrostatic energy calculation and a cutoff of 30 kcal/mol with smooth transition was used. Standard parameters were used for the generation of the CoMSIA fields. The PLS regression, using the experimental pIC₅₀ values as dependent variable, and the leave-one-out cross validation were performed in Sybyl. For CoMFA and CoMSIA, the CoMFA standard scaling and a column filtering of 2.0 kcal/mol were used. Gasteiger−Huckel charges were used for all ligands.

Molecular Descriptor-Based QSAR. Calculation of the molecular descriptors and PLS regressions were performed with the QuaSAR suite of applications of MOE using default parameters.[29] Experimental pIC₅₀ values were used as dependent variables. Gasteiger (PEOE) charges were used for all ligands.

Consensus Scoring. Consensus scoring was achieved by subjecting the pIC₅₀ predicted with the individual methodologies to PLS regression. The calculation was performed with the QuaSAR application of MOE.[29]

Chemistry. ¹H NMR spectra were obtained with a Varian Gemini-300 spectrometer (300 MHz) with D₂O, CDCl₃, CD₃OD, and DMSO-*d₆* as a solvent. Purity of the nucleosides was checked using a Hewlett-Packard 1100 HPLC equipped with a Luna 5*μ* RP-C18(2) analytical column (250 × 4.6 mm; Phenomenex, Torrance, CA). System B: linear gradient solvent system: CH₃CN/TBAP from 20/80 to 60/40 in 20 min, flow rate 1.0 mL/min. System C: linear gradient solvent system: CH₃CN/TBAP from 5/95 to 80/20 in 20 min, flow rate 1.0 mL/min. System D: linear gradient solvent system: H₂O/CH₃CN from 95/5 to 0/100 in 30 min; the flow rate was 1 mL/min. System E: linear gradient solvent system: H₂O/CH₃CN/AcOH from 90/10/0.05 to 50/50/0.05 in 40 min and 0/100/0.05 in 60 min, flow rate 0.5 mL/min. Peaks were detected by UV absorption with a diode array detector. All derivatives tested for biological activity showed ≥97% purity in the HPLC systems. Low-resolution and high-resolution FAB (fast atom bombardment) mass spectrometry was performed with a JEOL SX102 spectrometer with 6-kV Xe atoms following desorption from a glycerol matrix.

2,2-Dimethyl-propionic Acid 6-Chloro-2-cyanopurin-9-yl-methyl Ester (18). Pd₂(dba)₃−CHCl₃ (70 mg, 0.135 mmol) and tri-(2-furyl)phosphine (210 mg, 0.904 mmol) were dissolved in THF (0.3 mL) under dry N₂ atmosphere, and the solvent was removed under reduced pressure. 2,2-Dimethyl-propionic acid 6-chloro-2-iodopurin-9-ylmethyl ester[13] (333 mg, 0.814 mmol) and Zn(CN)₂ (450 mg, 3.83 mmol) in tetramethylurea (2.0 mL) were added, and the reaction mixture was stirred at 70 °C for 3 d. The crude reaction mixture was passed through a short silica gel column (eluted by AcOEt) to remove the salt and palladium, and the solvent was evaporated. The residue obtained was purified by silica gel column chromatography (AcOEt/petroleum ether = 1/2), which furnished **18** (156 mg, 63%). ¹H NMR (CDCl₃) δ 8.58 (s, 1H), 6.21 (s, 2H), 1.19 (s, 9H). MS (*m/e*) (positive-FAB) 294, 295 (peak ratio is 3:1) (M⁺ + H).

6-Methylamino-9*H*-purine-2-carbonitrile (19). To a solution of 2,2-dimethyl-propionic acid 6-chloro-2-cyanopurin-9-ylmethyl ester (**18**) (92 mg, 0.313 mmol) in MeCN (0.5 mL) was added 2 N MeNH₂ in THF (2.0 mL). The reaction mixture was stirred at rt for 2 d, and the solvent was removed under reduced pressure. The residue obtained was purified by recrystallization (from AcOEt), which furnished **6-methylamino-9*H*-purine-2-carbonitrile** (**19**, 21 mg, 39%). The filtrate was purified by silica gel column chromatography (AcOEt/petroleum ether=1/1), which furnished **2,2-dimethyl-propionic acid 2-cyano-6-methylaminopurin-9-yl-methyl ester** (**20**, 52.5 mg, 58%).

6-Methylamino-9*H*-purine-2-carbonitrile, 19. ¹H NMR (DMSO-*d₆*) δ 8.33 (s, 1H), 8.23 (bs, 1H), 2.96 (br, 3H). MS (*m/e*) (positive-FAB) 175 (M⁺ + H).

2,2-Dimethyl-propionic Acid 2-cyano-6-methylaminopurin-9-ylmethyl Ester, 20. ¹H NMR (CDCl₃) δ 8.13 (s, 1H), 6.11 (s, 2H), 5.65 (bs, 1H), 3.21 (br, 3H), 1.20 (s, 9H). MS (*m/e*) (positive-FAB) 289 (M⁺ + H).

(1′R,2′S,4′R,5′S)-Phosphoric Acid Di-*tert*-butyl Ester 4-(2-Cyano-6-methylaminopurin-9-yl)-1-(di-*tert*-butoxy-phosphoryl-oxymethyl)-bicyclo[3.1.0]hex-2-yl Ester (22). To a solution of triphenylphosphine (78 mg, 0.297 mmol) in anhydrous THF (0.50 mL) was added DIAD (0.060 mL, 0.305 mmol) at rt with stirring for 2 h. Compound **21**[13,15] (17 mg, 0.032 mmol) and 6-methylamino-2-cyano-9*H*-purine (13.5 mg, 0.78 mmol) in THF (0.8 mL) were added, and the reaction mixture was stirred at rt for 23 h. The solvent was removed under vacuum, and the residue obtained was purified by preparative thin-layer chromatography (AcOEt), which furnished **22** (6.0 mg, 27%). ¹H NMR (CDCl₃) δ 8.31 (s, 1H), 6.22 (bs, 1H), 5.34 (dd, 1H, *J* = 8.4, 14.5 Hz), 5.11 (d, 1H, *J* = 6.6 Hz), 4.68 (dd, 1H, *J* = 3.0, 9.6 Hz), 3.88 (dd, 1H, *J* = 6.6, 9.6 Hz), 3.20 (bs, 3H), 2.32 (dd, 1H, *J* = 8.4, 15.3 Hz), 2.11 (dd, 1H, *J* = 7.8, 15.3 Hz), 1.49 (s, 18H), 1.47 (s, 18H), 1.42 (m, 1H), 1.28

(m, 1H), 1.02 (m, 1H). MS (*m/e*) (positive-FAB) 685 (M$^+$ + H), 707 (M$^+$ + Na).

(1′R,2′S,4′R,5′S)-Phosphoric Acid Mono-[4-(2-cyano-6-methyl-aminopurin-9-yl)-1-phosphonooxymethyl-bicyclo[3.1.0]hex-2-yl] Ester (5), (1′R,2′S,4′R,5′S)-Phosphoric Acid Mono-[4-(2-car-bamoyl-6-methylaminopurin-9-yl)-1-phosphonooxymethyl-bicyclo-[3.1.0]hex-2-yl] Ester (6) and (1′R,2′S,4′R,5′S)-6-Methylamino-9-(4-phosphonooxy-5-phosphonooxymethyl-bicyclo[3.1.0]hex-2-yl)-9H-purine-2-carboxylic Acid (7). To a solution of **22** (6.0 mg, 0.0088 mmol) in CH$_2$Cl$_2$ (2.0 mL) was added TFA (0.100 mL), and the mixture was stirred at rt for 5.5 h. 2 N Et$_3$NH$_2$CO$_3$ buffer (2 mL) was added to the reaction mixture, and the crude product was lyophilized. Purification of the obtained residue was performed by an ion-exchange column packed with Sephadex-DEAE A-25 resin, a linear gradient (0.01 to 0.5 M) of ammonium bicarbonate was applied as the mobile phase, and UV and HPLC were used to monitor the elution, which furnished **5** (1.95 mg, 42%) and the mixture fraction of **5** and **6** (1:2 mixture, 2.0 mg).

The mixture fraction of **5** and **6** (1:2 mixture, 2.0 mg) was dissolved in H$_2$O (1.5 mL) and EtOH (1.5 mL). To this solution was added 3 N NaOH aq (0.5 mL) and 30% H$_2$O$_2$ aq (0.3 mL), and the reaction mixture was stirred at rt for 21 h and lyophilized. Purification of the obtained residue was performed by HPLC (a linear gradient of MeCN/TBAP = 20/80 to 80/20 in 15 min) and Sephadex-DEAE A-25 resin (a linear gradient 0.01M to 0.5 M of ammonium bicarbonate), to give **6** (0.67 mg, 14%) and **7** (1.32 mg, 27%).

(1′R,2′S,4′R,5′S)-Phosphoric Acid Mono-[4-(2-cyano-6-methyl-aminopurin-9-yl)-1-phosphonooxymethyl-bicyclo[3.1.0]hex-2-yl] Ester (5). ^{1}H NMR (D$_2$O) δ 8.64 (s, 1H), 5.08 (d, 1H, *J* = 6.6 Hz), 4.70−4.60 (m, 1H), 4.60−4.50 (m, 1H), 3.70 (m, 1H), 3.12 (s, 3H), 2.30(m, 1H), 2.02 (m, 1H), 1.93 (m, 1H), 1.23 (m, 1H),1.02 (t, 1H, *J* = 7.4 Hz). ^{31}P NMR (D$_2$O) δ 0.892 (s), 0.364 (s). MS (*m/e*) (negative-FAB) 459 (M$^+$ − H). LRMS (negative-FAB) calcd for C$_{14}$H$_{17}$N$_6$O$_8$P$_2$ 459.0583, found 459.058. HPLC 17.2 min (99%, System B), 2.3 min (99%, System D).

(1′R,2′S,4′R,5′S)-Phosphoric Acid mono-[4-(2-carbamoyl-6-methylaminopurin-9-yl)-1-phosphonooxymethyl-bicyclo[3.1.0]-hex-2-yl] Ester (6). ^{1}H NMR (D$_2$O) δ 8.63 (s, 1H), 5.30 (m, 1H), 5.20 (d, 1H *J* = 6.6 Hz), 4.58 (m, 1H), 3.46 (m, 1H), 3.20 (s, 3H), 2.28 (m, 1H), 2.03 (m, 1H), 1.87 (m, 1H), 1.34 (m, 1H), 1.21 (m, 1H). ^{31}P NMR (D$_2$O) δ 2.00 (s), 1.29 (s). MS (*m/e*) (negative-FAB) 477 (M$^+$ − H), 499 (M$^+$ − 2H + Na). HPLC 18.4 min (99%, System B), 3.8 min (99%, System D).

(1′R,2′S,4′R,5′S)-6-Methylamino-9-(4-phosphonooxy-5-phospho-nooxymethyl-bicyclo[3.1.0]hex-2-yl)-9H-purine-2-carboxylic Acid (7). ^{1}H NMR (D$_2$O) δ 8.69 (s, 1H), 5.27 (br, 1H), 5.19 (d, 1H, *J* = 6.0 Hz), 4.54 (m, 1H), 3.61 (m, 1H), 3.20 (s, 3H), 2.29(m, 1H), 2.01(m, 1H), 1.86(m, 1H),1.18(m, 1H), 0.96 (t, 1H, *J* = 7.4 Hz). ^{31}P NMR (D$_2$O) δ 2.82 (s), 2.14 (s). MS (*m/e*) (negative-FAB) 478 (M$^+$ − H). HPLC 16.0 min (99%, System B), 1.9 min (99%, System D).

(1′R,2′S,4′S,5′S)-Phosphoric Acid Di-*tert*-butyl Ester 1-(di-*tert*-butoxy-phosphoryloxymethyl)-4-(6-chloro-2-(2′-trimethyl-silyl)ethynylpurin-9-yl)-bicyclo[3.1.0]hex-2-yl Ester (24). To a solution of compound **23** (30 mg, 0.038 mmol) in 1.5 equiv of triethylamine solution were added trimethylsilylacetylene (0.01 mL, 0.0758 mmol), bis(triphenylphosphine)palladium(II) dichloride (2.6 mg, 0.1 equiv), and CuI (1.4 mg, 0.2 equiv) and stirred at room temperature for 7 h. The solvent was removed under vacuum, and the residue obtained was purified by preparative thin-layer chro-matography, which furnished product (20.5 mg, 71%). ^{1}H NMR (CDCl$_3$) 8.59 (s, 1H), 5.28 (d, *J* = 6.9 Hz, 1H), 5.26−5.33 (m, 2H), 4.69 (dd, *J* = 4.8, 11.4 Hz, 1H), 3.84 (dd, *J* = 6.3, 11.3 Hz, 1H), 2.30 (d, *J* = 8.4 Hz, 1H), 2.14−2.17 (m, 1H), 1.81−1.85 (m, 1H), 1.49 (s, 36H), 1.18 (dd, *J* = 3.9, 6.3 Hz, 1H), 1.02 (dd, *J* = 8.7, 6.0 Hz, 1H), 0.19 (s, 9H)

(1′R,2′S,4′S,5′S)-4-(2-Ethynyl-6-methylaminopurin-9-yl)-1-[(phosphato)-methyl]-2-(phosphato)-bicyclo[3.1.0]hexane (11). The mixture of **24** (33.0 mg, 0.043 mmol) in CH$_2$Cl$_2$ (3 mL) was

added TFA (0.1 mL), and the reaction mixture was stirred at room temperature for 3 h. After removal of the solvent, water (5.0 mL) was added in 40% MeNH$_2$ in water (1.0 mL) and stirred for 2 h at room temperature. The reaction was monitored by HPLC. The reaction mixture was subsequently frozen and lyophilized. Purifica-tion of the residue obtained was performed on an ion-exchange column packed with Sephadex-DEAE A-25 resin. A linear gradient (0.01−0.7 M) of ammonium bicarbonate was applied as the mobile phase, and UV and HPLC were used to monitor the elution, which furnished **11** (7.1 mg, 36%) ^{1}H NMR (CDCl$_3$) 8.65 (s, 1H), 5.05−5.11 (m, 1H), 4.96 (d, *J* = 6.6 Hz, 1H), 4.40 − 4.52 (m, 1H), 3.52−3.60 (m, 1H), 3.07 (bs, 4H), 2.17 − 2.23 (m, 1H), 1.81−1.88 (m, 2H), 1.10 − 1.13 (m, 1H), 0.92−0.93 (m, 1H) MS (*m/e*) (positive-FAB) 460 (M + H)$^+$.

2,2-Dimethyl-propionic Acid 6-Chloro-2-phenylpurin-9-yl-methyl Ester (25). Pd$_2$(dba)$_3$−CHCl$_3$ (9.5 mg, 9.17 μmol) and Ph$_3$P (19.0 mg, 72.4 μmol) were dissolved in THF (0.3 mL) under dry N$_2$ atmosphere, and the solvent was removed under reduced pressure. 2,2-Dimethyl-propionic acid 6-chloro-2-iodopurin-9-yl-methyl ester[13] (126 mg, 0.319 mmol), K$_2$CO$_3$ (71 mg, 0.514 mmol), PhB(OH)$_2$ (42 mg, 0.345 mmol), and toluene (1.0 mL) were added, and the reaction mixture was stirred at 100 °C for 7 d. The crude reaction mixture was passed through a short silica gel column (eluted by AcOEt) to remove the salt and palladium, and the solvent was evaporated. The residue obtained was purified by silica gel column chromatography (AcOEt/petroleum ether = 1/2), which furnished **25** (101 mg, 92%). ^{1}H NMR (CDCl$_3$) δ 8.55 (m, 2H), 8.34 (s, 1H), 7.51 (m, 3H), 6.26 (s, 2H), 1.19 (s, 9H). MS (*m/e*) (positive-FAB) 345, 347 (peak ratio is 3:1) (M$^+$ + H).

2,2-Dimethyl-propionic Acid 6-methylamino-2-phenylpurin-9-ylmethyl Ester (26). To a solution of 2,2-dimethyl-propionic acid 6-chloro-2-phenylpurin-9-ylmethyl ester (**25**) (90 mg, 0.261 mmol) in THF (3.0 mL) was added 2 N MeNH$_2$ in THF (1.0 mL). The reaction mixture was stirred at rt for 25 h, and the solvent was removed under reduced pressure. The residue obtained was purified by silica gel column chromatography (AcOEt/petroleum ether = 1/1 then 1/0), which furnished **26** (71 mg, 80%). ^{1}H NMR (CDCl$_3$) δ 8.53 (m, 2H), 7.98 (s, 1H), 7.51−7.41 (m, 3H), 6.19 (s, 2H), 5.89 (bs, 1H), 3.32 (bd, 3H, *J* = 4.8 Hz), 1.18 (s, 9H). MS (*m/e*) (positive-FAB) 340 (M$^+$ + H).

6-Methylamino-2-phenyl-9H-purine (27). To a solution of 2,2-dimethyl-propionic acid 6-methylamino-2-phenylpurin-9-ylmethyl ester (**26**) (58 mg, 0.172 mmol) in THF (1.0 mL) and MeOH (1.0 mL) was added 3 N NaOH aq (0.175 mL). The reaction mixture was stirred at rt for 3 h, and the solvent was removed under reduced pressure. The residue obtained was purified by silica gel column chromatography (AcOEt then CHCl$_3$/MeOH = 5/1), which fur-nished **27** (35 mg, 90%). ^{1}H NMR (DMSO-*d$_6$*) δ 8.40 (m, 2H), 7.94 (s, 1H), 7.47−7.35 (m, 3H), 3.07 (d, 3H, *J* = 4.5 Hz). MS (*m/e*) (positive-FAB) 226 (M$^+$ + H).

(1′R,2′S,4′R,5′S)-Phosphoric Acid Di-*tert*-butyl Ester 1-(Di-*tert*-butoxy-phosphoryloxymethyl)-4-(6-methylamino-2-phenyl-purin-9-yl)-bicyclo[3.1.0]hex-2-yl Ester (28). To a solution of triphenylphosphine (53 mg, 0.202 mmol) in anhydrous THF (0.50 mL) was added DIAD (0.035 mL, 0.178 mmol) at rt with stirring for 2 h. (1′R,2′S,4′R,5′S)-Phosphoric acid di-*tert*-butyl ester 1-(di-*tert*-butoxy-phosphoryloxymethyl)-4-hydroxy-bicyclo[3.1.0]hex-2-yl ester[13,15] (**21**, 25 mg, 0.48 mmol) and 6-methylamino-2-phenyl-9H-purine (46.5 mg, 0.206 mmol) in THF (1.0 mL) were added, and the reaction mixture was stirred at rt for 23 h. The solvent was removed under vacuum, and the residue obtained was purified by preparative thin-layer chromatography (AcOEt then chloroform/MeOH = 5/1), which furnished **28** (18 mg, 51%). ^{1}H NMR (CDCl$_3$) δ 8.52−8.48 (m, 2H), 8.09 (s, 1H), 7.49−7.40 (m, 3H), 5.88 (m, 1H), 5.41 (m, 1H), 5.27 (d, 1H, *J* = 7.2 Hz), 4.66 (dd, 1H, *J* = 4.5, 11.4 Hz), 3.90 (dd, 1H, *J* = 4.5, 11.4 Hz), 3.30 (bd, 3H, *J* = 5.1 Hz), 2.43 (m, 1H), 2.16 (m, 1H), 1.85 (m, 1H), 1.49 (s, 18H), 1.48 (s, 9H), 1.43 (s, 9H), 1.18 (m, 1H), 1.01(m, 1H). MS (*m/e*) (positive-FAB) 736 (M$^+$ + H).

(1′R,2′S,4′R,5′S)-Phosphoric Acid mono-[4-(6-methylamino-2-phenylpurin-9-yl)-1-phosphonooxymethyl-bicyclo[3.1.0]hex-

2-yl] Ester (13). To a solution of **28** (10.0 mg, 0.0136 mmol) in CH₂Cl₂ (2.0 mL) was added TFA (0.100 mL), and the mixture was stirred at rt for 2 d. 2 N Et₃NH₂CO₃ buffer (2 mL) was added to the reaction mixture, and the crude product was lyophilized. Purification of the obtained residue was performed by an ion-exchange column packed with Sephadex-DEAE A-25 resin, a linear gradient (0.01 to 0.5 M) of 0.5 M ammonium bicarbonate was applied as the mobile phase, and UV and HPLC were used to monitor the elution, which furnished **13** (3.6 mg, 46%). ^{1}H NMR (D₂O) δ 8.56 (bs, 1H), 8.04 (m, 2H), 7.61−7.50 (m, 3H), 5.25 (m, 1H), 5.09 (d, 1H, J = 6.0 Hz), 4.58 (dd, 1H, J = 4.2, 10.8 Hz), 3.72 (dd, 1H, J = 4.2, 10.8 Hz), 3.27 (bs, 3H), 2.33 (m, 1H), 2.05 (m, 1H), 1.85 (m, 1H), 1.23 (m, 1H), 1.03 (m, 1H). ^{31}P NMR (D₂O) δ 0.44 (bs). MS (*m/e*) (negative-FAB) 510 (M⁺ − H). HPLC 19.5 min (99%, System B), 16.2 min (99%, System C).

(1′R,2′S,4′S,5′S)-Acetic Acid 1-Acetoxymethyl-4-(6-chloro-2-iodopurin-9-yl)-bicyclo[3.1.0]hex-2-yl Ester (31). To a solution of triphenylphosphine (250 mg, 0.953 mmol) in anhydrous THF (1.00 mL) was added DEAD (0.150 mL, 0.953 mmol) at −78 °C, and the reaction mixture was stirred at rt for 0.5 h. Acetic acid 2-acetoxy-4-hydroxy-bicyclo[3.1.0]hex-1-ylmethyl ester[30] (**29**, 73 mg, 0.32 mmol) and 2-amino-6-chloropurine (**30**, 210 mg, 1.24 mmol) in THF (2.0 mL) were added, and the reaction mixture was stirred at rt for 4 d. The solvent was removed under vacuum, and the residue obtained was purified by silica gel column chromatography (chloroform then AcOEt/petroleum ether = 2/1). The residue obtained was dissolved in MeCN (1.00 mL), and diiodomethane (2.00 mL) and *tert*-butyl nitrite (0.30 mL, 3.3 mmol) were added. The tube was sealed after the nitrogen bubbling, and the reaction mixture was stirred at 80 °C for 3 h. The solvent was removed under reduced pressure. The residue obtained was purified by silica gel column chromatography (AcOEt/petroleum ether = 2/1), which furnished desired product (20.0 mg, 32%). ^{1}H NMR (CDCl₃) δ 8.40 (s, 1H), 5.68 (t, 1H, J = 8.5 Hz), 5.22 (d, 1H, J = 7.2 Hz), 4.68 (d, 1H, J = 12.0 Hz), 3.92 (d, 1H, J = 12.0 Hz), 2.42 (dd, 1H, J = 8.5, 15.6 Hz), 2.17 (s, 3H), 2.09 (s, 3H), 1.91 (m, 1H), 1.75 (dd, 1H, J = 4.2, 8.7 Hz), 1.18 (dd, 1H, J = 4.2, 8.7 Hz), 1.04 (m, 1H). MS (*m/e*) (positive-FAB) 491 (M⁺ + H).

(1′R,2′S,4′S,5′S)-1-Hydroxymethyl-4-(2-iodo-6-methylami-nopurin-9-yl)-bicyclo[3.1.0]hexan-2-ol (32). To a solution of acetic acid 1-acetoxymethyl-4-(6-chloro-2-iodopurin-9-yl)-bicyclo[3.1.0]-hex-2-yl ester (**31**, 20 mg, 0.041 mmol) in THF (0.030 mL) was added 2 N MeNH₂ in THF (0.30 mL), and the reaction mixture was stirred at rt for 6.5 h. MeOH (0.10 mL) and 3 N NaOH aq (0.040 mL) were added to the reaction mixture, which was stirred overnight at rt. The solvent was removed under vacuum, and the residue obtained was purified by silica gel column chromatography (AcOEt then CHCl₃/MeOH= 5/1), which furnished **32** (15 mg, 94%). ^{1}H NMR (CD₃OD) δ 8.36 (s, 1H), 4.96 (d, 1H, J = 6.6 Hz), 4.86 (t, 1H, J = 8.7 Hz), 4.25 (d, 1H, J = 11.7 Hz), 3.37 (d, 1H, J = 11.7 Hz), 3.05 (bs, 3H), 2.01 (m, 1H), 1.81 (m, 1H), 1.63 (dd, 1H, J = 3.6, 8.4 Hz), 1.01 (dd, 1H, J = 3.9, 5.7 Hz), 0.77 (dd, 1H, J = 6.0, 8.7 Hz). MS (*m/e*) (CI) 402 (M⁺ + H). HPLC 11.4 min (99%, System C), 31.5 min (99%, System E).

(1′R,2′S,4′S,5′S)-1-[Bis-(4-methoxy-phenyl)-phenyl-methoxy-methyl]-4-(2-iodo-6-methylaminopurin-9-yl)-bicyclo[3.1.0]hexan-2-ol (33). To a solution of 1-hydroxymethyl-4-(2-iodo-6-methyl-aminopurin-9-yl)-bicyclo[3.1.0]hexan-2-ol (**32**, 12 mg, 0.030 mmol) in DMF (0.50 mL) were added 4,4′-dimethoxytrityl chloride (47 mg, 0.139 mmol) and 4-dimethylaminopyridine (33 mg, 0.270 mmol), and the reaction mixture was stirred at rt for 24 h. The solvent was removed under vacuum, and the residue obtained was purified by silica gel column chromatography (AcOEt), which furnished **33** (19 mg, 92%). ^{1}H NMR (CDCl₃) δ 7.92 (s, 1H), 7.46−7.42 (m, 2H), 7.35−7.15 (m, 7H), 6.84 (d, 4H, J = 9.0 Hz), 5.76 (bs, 1H), 5.02 (d, 1H, J = 6.9 Hz), 4.94 (m, 1H), 3.53 (d, 1H, J = 9.9 Hz), 3.33 (d, 1H, J = 9.9 Hz), 3.17 (bs, 3H), 2.18−2.07 (m, 1H), 1.89−1.77 (m, 1H), 1.47 (m, 1H), 0.99 (m, 1H), 0.66 (m, 1H). MS (*m/e*) (positive-FAB) 704 (M⁺ + H).

(1′R,2′S,4′S,5′S)-Phosphoric Acid 1-[Bis-(4-methoxy-phenyl)-phenyl-methoxymethyl]-4-(2-iodo-6-methylaminopurin-9-yl)-

bicyclo[3.1.0]hex-2-yl Ester Di-*tert*-butyl Ester (34). Partial phosphorylation of the (N)-methanocarba ring was already reported.[12] To a stirred solution of **33** (18 mg, 0.026 mmol) and 1*H*-tetrazole (10 mg, 0.14 mmol) in anhydrous THF (0.25 mL) was added di-*tert*-butyl diethylphosphoramidite (0.035 mL, 0.13 mmol), and the mixture was stirred for 3.5 h at rt. The reaction mixture was cooled to −78 °C and treated with a solution of *m*-CPBA (70% max, 140 mg) in CH₂Cl₂ (2.0 mL). The resulting mixture was warmed up to rt and stirred for 30 min. 5% NaHSO₃ (2.0 mL) was added to the reaction mixture and stirred another 10 min at rt. The reaction mixture was extracted with AcOEt, and the organic phase was subsequently washed with sat. aq NaHCO₃ and brine, dried over Na₂SO₄, and filtered. The solvent was removed under reduced pressure. The obtained residue was purified by silica gel column chromatography (AcOEt/petroleum ether = 1/1 to 1/0 then CHCl₃/MeO = 5/1), to give **34** (4.7 mg, 21%). ^{1}H NMR (CDCl₃) δ 8.08 (s, 1H), 7.41−7.37 (m, 2H), 7.36−7.16 (m, 7H), 6.79 (d, 4H, J = 8.1 Hz), 5.91 (bs, 1H), 5.51 (m, 1H), 5.05 (d, 1H, J = 6.9 Hz), 3.95 (d, 1H, J = 9.9 Hz), 3.78 (s, 6H), 3.61 (bs, 3H), 2.98 (d, 1H, J = 9.9 Hz), 2.36−2.27 (m, 1H), 2.10−1.95 (m, 1H), 1.47 (m, 1H), 1.42 (s, 9H), 1.39 (s, 9H), 0.94 (m, 1H), 0.80 (m, 1H). MS (*m/e*) (positive-FAB) 896 (M⁺ + H).

(1′R,2′S,4′S,5′S)-Phosphoric Acid mono-[1-hydroxymethyl-4-(2-iodo-6-methylaminopurin-9-yl)-bicyclo[3.1.0]hex-2-yl] Ester (14). To a solution of **34** (4.7 mg, 0.0052 mmol) in CH₂Cl₂ (2.0 mL) was added TFA (0.100 mL), which was stirred at rt for 3 h. 2 N Et₃NH₂CO₃ buffer (2 mL) was added to the reaction mixture, and the crude product was lyophilized. Purification of the obtained residue was performed by an ion-exchange column packed with Sephadex-DEAE A-25 resin, a linear gradient (0.01 to 0.5 M) of ammonium bicarbonate was applied as the mobile phase, and UV and HPLC were used to monitor the elution, which furnished **14** (1.70 mg, 63%). ^{1}H NMR (D₂O) δ 8.23 (s, 1H), 5.21 (dd, 1H, J = 8.1, 15.6 Hz), 4.95 (d, 1H, J = 6.9 Hz), 4.12 (d, 1H, J = 12.6 Hz), 3.58 (d, 1H, J = 12.6 Hz), 3.08 (bs, 3H), 2.32 (dd, 1H, J = 8.1, 15.0 Hz), 2.05 (dd, 1H, J = 7.8, 15.0 Hz), 1.82 (m, 1H), 1.17 (m, 1H), 0.96 (m, 1H). ^{31}P NMR (D₂O) δ 0.465 (s). MS (*m/e*) (negative-FAB) 480 (M⁺ − H). HPLC 13.7 min (>99%, System B).

[3-(2-Iodo-6-chloropurin-9-yl)-2-(diethoxyphosphorylmethyl)-propyl]-phosphonic Acid Diethyl Ester (37). The starting alcohol tetraethyl 2-hydroxymethyl-1,3-propanebisphosphonate (**36**) was dried by coevaporation from anhydrous THF (10 mL) two times. Subsequently, a solution of **36** (0.064 g, 0.2 mmol) in anhydrous THF (10 mL) was combined with 2-iodo-6-chloropurine **35** (0.112 g, 0.4 mmol), triphenylphosphine (0.104 g, 0.4 mmol), and diethyl azodicarboxylate (0.068 g, 0.4 mmol) and stirred at ambient temperature overnight. The solution was concentrated, and the resulting residue was purified by purified by preparative thin layer chromatography by using chloroform/methanol (9:1) as solvent to provide **37** (0.062 g, 52%). ^{1}H NMR (400 MHz, CDCl₃) δ 1.34 (t, J = 6.1 Hz, 12H), 1.80−2.08 (m, 4H), 2.95 (m, 1H), 4.05−4.21 (m, 8H), 4.60 (d, J = 6.0 Hz, 2H), 8.38 (s, 1H); ^{31}P NMR (162 MHz, CDCl₃) δ 31.1; TOFMS *m/z* 609.2 (M + H⁺).

[3-(2-Iodo-6-methylaminopurin-9-yl)-2-(diethoxyphosphoryl-methyl)-propyl]-phosphonic Acid Diethyl Ester (38). A THF (2 mL) solution of **37** (0.061 g, 0.1 mmol) and 40% methylamine (0.12 mL, 1.7 mmol) was stirred at ambient temperature for 1 h. The reaction solution was concentrated, and the residue was purified directly by preparative thin layer chromatography by using chloroform/methanol (9:1) as solvent to furnish **38** (0.044 g, 74%). ^{1}H NMR (400 MHz, CDCl₃) δ 1.34 (t, 12H, J = 7.2 Hz), 1.81−2.05 (m, 4H), 2.92 (m, 1H), 3.41 (s, 3H), 4.12 (m, 8H), 4.43 (d, J = 4.9 Hz, 2H), 8.04 (s, 1H); ^{31}P NMR (162 MHz, CDCl₃) δ 29.2; TOFMS *m/z* 604.2 (M + H⁺).

[3-(2-Iodo-6-methylaminopurin-9-yl)-2-phosphonomethylpro-pyl]-phosphonic Acid Tetraammonium Salt (16). Compound **38** (0.120 g, 0.2 mmol) was dissolved into anhydrous acetonitrile (4 mL). Iodotrimethylsilane (0.2 mL, 1.35 mmol) was added. The reaction was stirred at ambient temperature for 4.5 h. Then reaction was concentrated to dryness. The residue was added with triethylammonium bicarbonate buffer (0.2 mL) followed by water

(10 mL), and the solution was extracted with diethyl ether (3 mL × 5). The aqueous layer was concentrated under reduced pressure. The residue was purified by ion-exchange column chromatography using Sephadex-DEAE A-25 resin with a linear gradient (0.01– 0.5 M) of ammonium bicarbonate as mobile phase to give 46 mg of **16** as a pale yellow solid (42%). ^{1}H NMR (400 MHz, D$_2$O) δ 1.61–1.78 (m, 2H), 1.84–1.98 (m, 2H), 2.67 (m, 1H), 3.06 (s, 3H), 4.47 (d, *J* = 5.4 Hz, 2H), 8.31 (d, 1H, *J* = 6.0 Hz); ^{31}P NMR (162 MHz, D$_2$O) δ 23.4; TOFMS *m/z* 490.1 (M– H$^+$).

Pharmacology. 2-MeSADP was purchased from Sigma (St. Louis, MO). Myo-[^{3}H]inositol (20 Ci/mmol) was obtained from American Radiolabeled Chemicals (St. Louis, MO).

P2Y receptor-promoted stimulation of inositol phosphate formation was measured at the human P2Y$_1$ receptor stably expressed in 1321N1 human astrocytoma cells as previously described.[35,36] The IC$_{50}$ values were averaged from three independently determined concentration-effect curves for each compound. Briefly, cells plated in 24-well dishes were labeled in inositol-free medium (DMEM; Gibco, Gaithersburg, MD) containing 1.0 μCi of 2-[^{3}H]*myo*-inositol for 18–24 h in a humidified atmosphere of 95% air/5% CO$_2$ at 37 °C. PLC activity was measured the following day by quantitating [^{3}H]inositol phosphate accumulation after a 10 min incubation at 37 °C in the presence of 10 mM LiCl. Total [^{3}H]inositol phosphates were quantified by anion exchange chromatography as previously described.[35,36] The affinities of bisphosphate analogues for the human P2Y$_1$ receptor were directly determined by using [^{3}H]**3b** in a radioligand binding assay, as we recently described in detail.[37] Binding and functional parameters were estimated using GraphPAD Prism software (GraphPAD, San Diego, CA).

Supporting Information Available: A table reporting the structures of all the compounds in the training set, their potencies, and references to the original publications (Table S1); a table reporting the MOE QSAR prediction of the potency of the test set compounds after addition of compound **6** or compound **7** to the training set (Table S2); plots of experimental vs calculated potencies for the 45 compounds of the training set (Figure S1); enlarged versions of all the panels of Figure 1 and Figure 2 (Figure S2); plots of experimental vs calculated potencies for the eight compounds of the test set (Figure S3); synoptic view of experimental vs calculated potencies for the eight compounds of the test set (Figure S4); a table reporting the purity of the target compounds as measured by HPLC. This material is available free of charge via the Internet at http://pubs.acs.org.

References

(1) Costanzi, S.; Mamedova, L.; Gao, Z. G.; Jacobson, K. A. Architecture of P2Y nucleotide receptors: structural comparison based on sequence analysis, mutagenesis, and homology modeling. *J. Med. Chem.* **2004**, *47*, 5393–5404.

(2) Abbracchio, M. P.; Burnstock, G.; Boeynaems, J. M.; Barnard, E. A.; Boyer, J. L.; Kennedy, C.; Knight, G. E.; Fumagalli, M.; Gachet, C.; Jacobson, K. A.; Weisman, G. A. International Union of Pharmacology LVIII: update on the P2Y G protein-coupled nucleotide receptors: from molecular mechanisms and pathophysiology to therapy. *Pharmacol. Rev.* **2006**, *58*, 281–341.

(3) Gachet, C.; Hechler, B. The platelet *P2* receptors in thrombosis. *Semin. Thromb. Hemostasis* **2005**, *31*, 162–167.

(4) Jin, J.; Kunapuli, S. P. Coactivation of two different G protein-coupled receptors is essential for ADP-induced platelet aggregation. *Proc. Natl. Acad. Sci. U.S.A.* **1998**, *95*, 8070–8074.

(5) Savi, P.; Herbert, J. M. Clopidogrel and ticlopidine: P2Y$_{12}$ adenosine diphosphate-receptor antagonists for the prevention of atherothrombosis. *Semin. Thromb. Hemostasis* **2005**, *31*, 174–183.

(6) Hechler, B.; Nonne, C.; Roh, E. J.; Cattaneo, M.; Cazenave, J. P.; Lanza, F.; Jacobson, K. A.; Gachet, C. MRS2500 [2-iodo-N^6-methyl-(N)-methanocarba-2′-deoxyadenosine-3′,5′-bisphosphate], a potent, selective, and stable antagonist of the platelet P2Y$_1$ receptor with strong antithrombotic activity in mice. *J. Pharmacol. Exp. Ther.* **2006**, *316*, 556–563.

(7) Boyer, J. L.; Romero-Avila, T.; Schachter, J. B.; Harden, T. K. Identification of competitive antagonists of the P2Y$_1$ receptor. *Mol. Pharmacol.* **1996**, *50*, 1323–1329.

(8) Camaioni, E.; Boyer, J. L.; Mohanram, A.; Harden, T. K.; Jacobson, K. A. Deoxyadenosine bisphosphate derivatives as potent antagonists at P2Y$_1$ receptors. *J. Med. Chem.* **1998**, *41*, 183–190.

(9) Nandanan, E.; Camaioni, E.; Jang, S. Y.; Kim, Y. C.; Cristalli, G.; Herdewijn, P.; Secrist, J. A., III; Tiwari, K. N.; Mohanram, A.; Harden, T. K.; Boyer, J. L.; Jacobson, K. A. Structure–activity relationships of bisphosphate nucleotide derivatives as P2Y$_1$ receptor antagonists and partial agonists. *J. Med. Chem.* **1999**, *42*, 1625–1638.

(10) Nandanan, E.; Jang, S. Y.; Moro, S.; Kim, H. O.; Siddiqui, M. A.; Russ, P.; Marquez, V. E.; Busson, R.; Herdewijn, P.; Harden, T. K.; Boyer, J. L.; Jacobson, K. A. Synthesis, biological activity, and molecular modeling of ribose-modified deoxyadenosine bisphosphate analogues as P2Y$_1$ receptor ligands. *J. Med. Chem.* **2000**, *43*, 829–842.

(11) Kim, H. S.; Barak, D.; Harden, T. K.; Boyer, J. L.; Jacobson, K. A. Acyclic and cyclopropyl analogues of adenosine bisphosphate antagonists of the P2Y$_1$ receptor: structure–activity relationships and receptor docking. *J. Med. Chem.* **2001**, *44*, 3092–3108.

(12) Xu, B.; Stephens, A.; Kirschenheuter, G.; Greslin, A. F.; Cheng, X.; Sennelo, J.; Cattaneo, M.; Zighetti, M. L.; Chen, A.; Kim, S. A.; Kim, H. S.; Bischofberger, N.; Cook, G.; Jacobson, K. A. Acyclic analogues of adenosine bisphosphates as P2Y receptor antagonists: phosphate substitution leads to multiple pathways of inhibition of platelet aggregation. *J. Med. Chem.* **2002**, *45*, 5694–5709.

(13) Kim, H. S.; Ohno, M.; Xu, B.; Kim, H. O.; Choi, Y.; Ji, X. D.; Maddileti, S.; Marquez, V. E.; Harden, T. K.; Jacobson, K. A. 2-Substitution of adenine nucleotide analogues containing a bicyclo-[3.1.0]hexane ring system locked in a northern conformation: enhanced potency as P2Y$_1$ receptor antagonists. *J. Med. Chem.* **2003**, *46*, 4974–4987.

(14) Ohno, M.; Costanzi, S.; Kim, H. S.; Kempeneers, V.; Vastmans, K.; Herdewijn, P.; Maddileti, S.; Gao, Z. G.; Harden, T. K.; Jacobson, K. A. Nucleotide analogues containing 2-oxa-bicyclo[2.2.1]heptane and l-alpha-threofuranosyl ring systems: interactions with P2Y receptors. *Bioorg. Med. Chem.* **2004**, *12*, 5619–5630.

(15) Cattaneo, M.; Lecchi, A.; Ohno, M.; Joshi, B. V.; Besada, P.; Tchilibon, S.; Lombardi, R.; Bischofberger, N.; Harden, T. K.; Jacobson, K. A. Antiaggregatory activity in human platelets of potent antagonists of the P2Y$_1$ receptor. *Biochem. Pharmacol.* **2004**, *68*, 1995–2002.

(16) Houston, D.; Ohno, M.; Nicholas, R. A.; Jacobson, K. A.; Harden, T. K. [^{32}P]2-iodo-N$_6$-methyl-(N)-methanocarba-2′-deoxyadenosine-3′,5′-bisphosphate ([^{32}P]MRS2500), a novel radioligand for quantification of native P2Y$_1$ receptors. *Br. J. Pharmacol.* **2006**, *147*, 459–467.

(17) Palczewski, K.; Kumasaka, T.; Hori, T.; Behnke, C. A.; Motoshima, H.; Fox, B. A.; Le, T., I; Teller, D. C.; Okada, T.; Stenkamp, R. E.; Yamamoto, M.; Miyano, M. Crystal structure of rhodopsin: A G protein-coupled receptor. *Science* **2000**, *289*, 739–745.

(18) Moro, S.; Guo, D.; Camaioni, E.; Boyer, J. L.; Harden, T. K.; Jacobson, K. A. Human P2Y$_1$ receptor: molecular modeling and site-directed mutagenesis as tools to identify agonist and antagonist recognition sites. *J. Med. Chem.* **1998**, *41*, 1456–1466.

(19) Ferrara, P.; Gohlke, H.; Price, D. J.; Klebe, G.; Brooks, C. L., III. Assessing scoring functions for protein–ligand interactions. *J. Med. Chem.* **2004**, *47*, 3032–3047.

(20) Warren, G. L.; Andrews, C. W.; Capelli, A. M.; Clarke, B.; LaLonde, J.; Lambert, M. H.; Lindvall, M.; Nevins, N.; Semus, S. F.; Senger, S.; Tedesco, G.; Wall, I. D.; Woolven, J. M.; Peishoff, C. E.; Head, M. S. A Critical Assessment of Docking Programs and Scoring Functions. *J. Med. Chem.* **2006**, *49*, 5912–5931.

(21) Costanzi, S.; Joshi, B. V.; Maddileti, S.; Mamedova, L.; Gonzalez-Moa, M. J.; Marquez, V. E.; Harden, T. K.; Jacobson, K. A. Human P2Y$_6$ receptor: molecular modeling leads to the rational design of a novel agonist based on a unique conformational preference. *J. Med. Chem.* **2005**, *48*, 8108–8111.

(22) Chang, G.; Guida, W. C.; Still, W. C. An Internal Coordinate Monte Carlo Method for Searching Conformational Space. *J. Am. Chem. Soc.* **1989**, *111*, 4379–4386.

(23) Glide. [4.0]. 2005. Schrödinger, LLC. ref Type: Computer Program.

(24) Aqvist, J.; Medina, C.; Samuelsson, J. E. A new method for predicting binding affinity in computer-aided drug design. *Protein Eng* **1994**, *7*, 385–391.

(25) Jones-Hertzog, D. K.; Jorgensen, W. L. Binding affinities for sulfonamide inhibitors with human thrombin using Monte Carlo simulations with a linear response method. *J. Med. Chem.* **1997**, *40*, 1539–1549.

(26) Liaison. [4.0]. 2005. Schrödinger, LLC. Ref Type: Computer Program.

(27) Zhou, R.; Friesner, R. A.; Ghosh, A.; Rizzo, R. C.; Jorgensen, W. L.; Levy, R. M. New Linear Interaction Method for Binding Affinity Calculations Using a Continuum Solvent Model. *J. Phys. Chem. B* **2001**, *105*, 10388−10397.

(28) Singh, P.; Mhaka, A. M.; Christensen, S. B.; Gray, J. J.; Denmeade, S. R.; Isaacs, J. T. Applying linear interaction energy method for rational design of noncompetitive allosteric inhibitors of the sarco- and endoplasmic reticulum calcium-ATPase. *J. Med. Chem.* **2005**, *48*, 3005−3014.

(29) MOE. [2005.06]. 2005. Chemical Computing Group Inc. Ref Type: Computer Program.

(30) Yoshimura, Y.; Moon, H. R.; Choi, Y.; Marquez, V. E. Enantiose-lective synthesis of bicyclo[3.1.0]hexane carbocyclic nucleosides via a lipase-catalyzed asymmetric acetylation. Characterization of an unusual acetal byproduct. *J. Org. Chem.* **2002**, *67*, 5938−5945.

(31) Tchilibon, S.; Joshi, B. V.; Kim, S. K.; Duong, H. T.; Gao, Z. G.; Jacobson, K. A. (N)-methanocarba 2,N⁶-disubstituted adenine nucleo-sides as highly potent and selective A₃ adenosine receptor agonists. *J. Med. Chem.* **2005**, *48*, 1745−1758.

(32) MacroModel. [9.1]. 2005. Schrödinger, LLC. Ref Type: Computer Program.

(33) Mohamadi, F.; Richards, N. G. J.; Guida, W. C.; Liskamp, R.; Lipton, M.; Caufield, C.; Chang, G.; Hendrickson, T.; Still, W. C. Macro-model - An Integrated Software System for Modeling Organic and Bioorganic Molecules Using Molecular Mechanics. *J. Comput. Chem.* **1990**, *11*, 440−467.

(34) Friesner, R. A.; Murphy, R. B.; Repasky, M. P.; Frye, L. L.; Greenwood, J. R.; Halgren, T. A.; Sanschagrin, P. C.; Mainz, D. T. Extra precision glide: docking and scoring incorporating a model of hydrophobic enclosure for protein−ligand complexes. *J. Med. Chem.* **2006**, *49*, 6177−6196.

(35) Harden, T. K.; Hawkins, P. T.; Stephens, L.; Boyer, J. L.; Downes, C. P. hosphoinositide hydrolysis by guanosine 5′-[gamma-thio]-triphosphate-activated phospholipase C of turkey erythrocyte mem-branes. *Biochem. J.* **1988**, *252*, 583−593.

(36) Boyer, J. L.; Downes, C. P.; Harden, T. K. Kinetics of activation of phospholipase C by P2Y purinergic receptor agonists and guanine nucleotides. *J. Biol. Chem.* **1989**, *264*, 884−890.

(37) Waldo, G. L.; Corbitt, J.; Boyer, J. L.; Ravi, G.; Kim, H. S.; Ji, X. D.; Lacy, J.; Jacobson, K. A.; Harden, T. K. Quantitation of the P2Y₁ receptor with a high affinity radiolabeled antagonist. *Mol. Pharmacol.* **2002**, *62*, 1249−1257.

(38) Labute, P. A widely applicable set of descriptors. *Journal of Molecular Graphics Modeling* **2000**, *18*, 464−477.

(39) Wildman, S. A.; Crippen, G. M. Prediction of physicochemical parameters by atomic contributions. *J. Chem. Inf. Comput. Sci.* **1999**, *39*, 868−873.

(40) Ertl, P.; Rohde, B.; Selzer, P. Fast calculation of molecular polar surface area as a sum of fragment-based contributions and its application to the prediction of drug transport properties. *J. Med. Chem.* **2000**, *43*, 3714−3717.

(41) Hou, T. J.; Xia, K.; Zhang, W.; Xu, X. J. ADME evaluation in drug discovery. 4. Prediction of aqueous solubility based on atom contribution approach. *J. Chem. Inf. Comput. Sci.* **2004**, *44*, 266−275.

(42) Kier, L. B.; Hall, L. H. Nature of Structure−activity-Relationships and Their Relation to Molecular Connectivity. *Eur. J. Med. Chem.* **1977**, *12*, 307−312.